



4

6

7

8

9

10

11 12

13

14

15

16 17

18

19

20

21

22

23

24

25

26

27

28

29

30

31

32

33

35

36

37

38

39

40

41

42

43

44

45

Article

# A label-free electrical impedance spectroscopy for detection of small extracellular vesicles based on their unique dielectric properties

Yuqian Zhang <sup>1,2</sup>, Kazutoshi Murakami <sup>3</sup>, Vishnupriya J Borra <sup>3</sup>, Mehmet Ozgun Ozen <sup>4</sup>, Utkan Demirci <sup>4</sup>, Takahisa Nakamura <sup>3,5,6</sup>, Leyla Esfandiari <sup>7,8,9\*</sup>

- Department of Surgery, Division of Surgical Research, Mayo Clinic, Rochester, MN, USA; zhang.yuqian@mayo.edu
- <sup>2</sup> Microbiome Program, Center for Individualized Medicine, Mayo Clinic, Rochester, MN, USA
- <sup>3</sup> Division of Endocrinology, Cincinnati Children's Hospital Medical Center, Cincinnati, OH, USA; <u>kazumurakami@okayama-u.ac.jp</u> (K.M.); <u>vishnupriya.borra@cchmc.org</u> (V.J.B.); <u>takahisa.nakamura@cchmc.org</u> (T.K.)
- <sup>4</sup> Canary Center at Stanford for Cancer Early Detection, Department of Radiology, Stanford School of Medicine, Stanford University, Palo Alto, CA, USA; <a href="mailto:mehmeto@stanford.edu">mehmeto@stanford.edu</a> (M.O.O.); <a href="mailto:utkan@stanford.edu">utkan@stanford.edu</a> (U.D.)
- Department of Pediatrics, College of Medicine, University of Cincinnati, Cincinnati, OH, USA
- <sup>6</sup> Department of Metabolic Bioregulation, Institute of Development, Aging and Cancer, Tohoku University, Japan
- Department of Biomedical Engineering, College of Engineering and Applied Sciences, University of Cincinnati, Cincinnati, OH, USA; <a href="mailto:esfandla@ucmail.uc.edu">esfandla@ucmail.uc.edu</a>
- Bepartment of Electrical Engineering and Computer Science, College of Engineering and Applied Sciences, University of Cincinnati, Cincinnati, OH, USA
- 9 Department of Environmental and Public Health Sciences, University of Cincinnati, Cincinnati, OH, USA
- Correspondence: esfandla@ucmail.uc.edu

Abstract: Extracellular vesicles (EVs) have gained excessive attention as vital circulating biomarkers since their structure and composition resemble the originating cells. The investigation of EVs' biochemical and biophysical properties is of great importance to map them to their parental cells and to better understand their functionalities. In this study, a novel frequency-dependent impedance measurement system has been developed to characterize EVs based on their unique dielectric properties. The system is composed of an insulator-based dielectrophoretic (iDEP) device to entrap and immobilize vesicles followed by utilizing an electrical impedance spectroscopy (EIS) to measure their impedance at a wide frequency spectrum, aiming to analyze both their membrane and cytosolic charge-dependent contents. The EIS was initially utilized to detect nano-size vesicles with different biochemical compositions, including liposomes synthesized with different lipid compositions, as well as EVs and lipoproteins with alike biophysical properties but dissimilar biochemical properties. Moreover, EVs derived from same parental cells but treated with different culture conditions were characterized to investigate the correlation of impedance changes to biochemical properties and functionality in terms of pro-inflammatory responses. The system also showed the ability to discriminate between EVs derived from different cellular origins, as well as among size-sorted EVs harbored from the same cellular origin. This proof-of-concept approach is the first step towards utilizing EIS as a label-free, non-invasive, and rapid sensor for detection of pathogenic EVs and other nanovesicles in the future.

Citation: Lastname, F.; Lastname, F.; Lastname, F. Title. *Biosensors* **2022**, 12, x. https://doi.org/10.3390/xxxxx

Received: date Accepted: date Published: date

**Publisher's Note:** MDPI stays neutral with regard to jurisdictional claims in published maps and institutional affiliations.



Copyright: © 2021 by the authors. Submitted for possible open access publication under the terms and conditions of the Creative Commons Attribution (CC BY) license (https://creativecommons.org/license s/by/4.0/).

**Keywords:** Extracellular vesicles (EVs), Exosome, dielectric properties, electrical impedance spectroscopy (EIS), insulator-based dielectrophoretic (iDEP), biosensor

# 1. Introduction

Extracellular vesicles (EVs), including exosomes (40-150 nm) and microvesicles are released from many cell types into extracellular space and are circulated in almost all

biofluids including blood, urine, breast milk, cerebral fluids, and saliva [1]. They are taken up by neighboring or distant cells and subsequently modulate functions of the recipient cells. EVs are composed of a lipid bilayer membrane containing unique receptors and tetraspanin surface markers. They also encapsulate exclusive cargos in their lumen, including proteins, lipids, and nucleic acids [2]. The unique composition of EVs reflects their parental cells with both physiological and pathological relevance [3]. Thus, detection and characterization of EVs surface markers and cargos offers great opportunity for early diagnosis and monitoring the prognosis of several diseases including cancer, cardiovascular disease and degenerative disorders [4]. The state-of-the-art technologies are mainly based on EVs' biophysical characterization including their size distribution, density, and morphology; and can be listed as transmission electron microscopy (TEM) [5], nanoparticle tracking analysis (NTA) [6], and density gradient separation [7]. However, these techniques are either low throughput and time-consuming to operate, or do not provide information with regards to EV's biochemical properties, cellular origins, and functionality. Thus, in recent years, flow cytometry has been adopted as a high-throughput method for characterization of EVs based on their biochemical properties by labeling their specific protein markers, their membrane lipids, or nucleic acids [8]. Although flow cytometry has shown promising attributes, it is a label-based technique which relies on the specificity of antibodies to the targeted receptors. More importantly, the flow cytometry lacks accuracy for characterization of EVs with smaller size distribution since the scatter sensitivity of current technologies is limited to EVs larger than ~100 nm [9]. Other analytical methods, such as western blot, mass-spectrometry (MS), microarray technology and RNA sequencing, are applied to study the abundance of EVs' proteins, lipids, and nucleic acids [10]. Although these techniques are highly sensitive for EVs' biochemical profiling, they require lysis or labeling steps prior to screening, which not only add time and cost to the procedure, but also break the structure of the vesicles; Considering the therapeutic potential of EVs, it is important to maintain EVs intact structure and native composition.

Electrical impedance spectroscopy (EIS) is a label-free and non-invasive technology that has been developed for measuring the impedance of cells under an alternating current (AC) over a wide range of frequency, aiming to characterize their dielectric properties which resemble their unique membrane and cytosolic compositions [11,12]. This technique has been widely utilized to differentiate stem cells [13] and cancerous cells [14]. In majority of EIS techniques, a single cell is initially trapped at a fixed position, followed by impedance measurement of the cell at a selected frequency range [15]. The variation of impedance signal provides information on cells' morphological and electrophysiological changes which are related to the cells' intrinsic dielectric properties. Microfluidic flow cytometry (MFC) is another impedance-based cellular analysis, in which a single cell dynamically flows through a channel with embedded micro-electrodes. The impedance of a cell at a wide frequency spectrum is collected for the analysis of its properties including size, membrane capacitance and cytoplasmic conductance [16,17]. However, the application of the EIS tools for detection of EVs with heterogeneous and nanoscale size distribution has not been explored.

In this proof-of-concept study, we have adopted EIS to detect a cluster of EVs harvested from different cellular origins, and investigated the correlation between their impedance responses to their intrinsic dielectric properties, including their unique membrane and cytosolic characteristics. EVs were first immobilized by an iDEP device developed by our team [18,19], followed by sweeping an AC field at 100 mVrms from 0.5 MHz to 50 MHz for impedance measurements by an integrated EIS, as illustrated in Figure 1a. We have initially detected liposomes and carboxylic acid polystyrene (COOH-PS) beads of similar size with known dielectric properties, followed by constructing an equivalent circuit model for theoretical validation. The system has further been utilized to characterize different EVs with different membrane properties as well as treating them with different stimulus in culture (Figure 1b i) to obtain the impedance responses to variation of their membrane and cytosolic dielectrics at a wide range of frequency. Moreover, we utilized

102

103

104

105

106

107

108

109

110

111

112

113

114

115

116

117

118

119

120

121

122

123

124

125

126

127

128

129

130

131

132

133

134

the system to differentiate EVs from lipoproteins, detect EVs derived from different cellular origins ((Figure 1b i); and EVs secreted from same cellular origins but different size ranges (Figure 1b iii). Overall, this approach established a rapid and label-free detection scheme for characterization of EVs with different biochemical compositions and potentially functionality; laying the foundation to leverage EVs as circulating biomarkers for disease diagnosis and prognosis or as personalized therapeutic cargos.

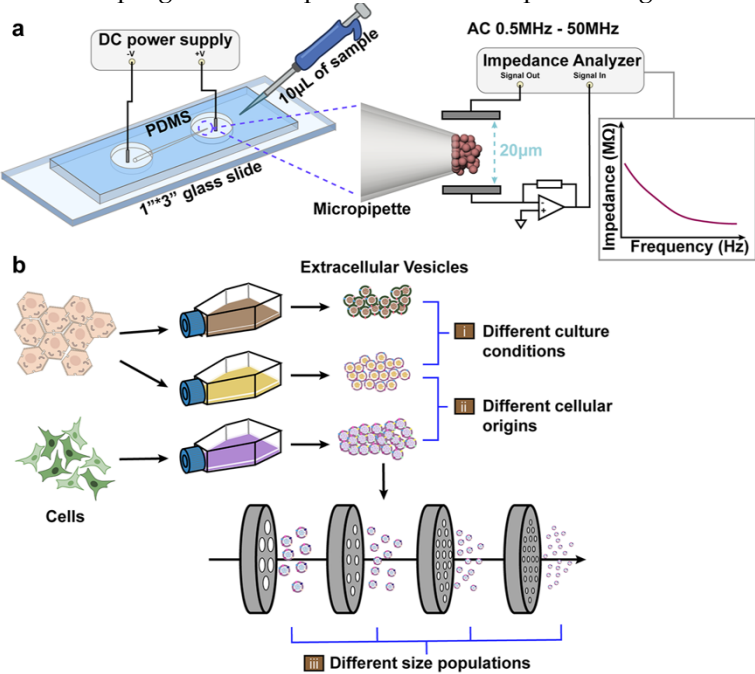


**Figure 1. (a)** Schematic of an integrated iDEP and EIS system. The setup composed of a borosilicate micropipette placed in between two PDMS chambers where DC bias was applied to trap vesicles at the pipettes' tip by electrokinetic forces. Followed by measuring the impedance of the collected vesicles utilizing the sensing electrodes, at a wide frequency spectrum (0.5 MHz to 50 MHz). **(b)** Detection of EVs harvested from: **i)** cells under different culture conditions, **ii)** different cellular origins, and **iii)** different size population.

## 2. Materials and Methods

Materials. All chemicals were purchased from Sigma-Aldrich (St. Louis, MO, USA) unless otherwise noted. Silicone elastomer base and curing agents were purchased from Dow Corning (Elizabethtown, KY, USA). Platinum electrodes were purchased from Alfa Aesar (Haverhill, MA, USA). Phosphate-buffered saline (PBS) was purchased from Roche Diagnostics (Indianapolis, IN, USA). Borosilicate pipettes with filament (O.D. 1 mm; I.D. 0.78 mm; length 7.5 cm) were obtained from Sutter Instrument (Novato, CA, USA). 100 nm liposomes (phospholipid DOPC and cholesterol) were purchased from FormuMax Scientific Inc. (Sunnyvale, CA, USA). 100 nm COOH-PS beads were obtained from Bangs Laboratories, Inc. (Fisher, IN, USA). EVs derived from A549 non-small cell lung cancer (NSCLC) were purchased from ATCC (Manassas, VA, USA). Dulbecco's Modified Eagle Medium (DMEM), Antibiotic-Antimycotic (Anti-Anti), and Exosome-depleted Fetal Bovine Serum were purchased from Thermo Fisher scientific (Waltham, MA, USA). Fetal Bovine Serum (regular) was purchased from Hyclone Laboratories Inc. (Logan, UT, USA). MagCapture Exosome Isolation Kit PS was purchased from FUJIFILM Wako Pure Chemical Corp. (Richmond, VA, USA). N,N'-Bis[4-(4,5-dihydro-1H-imidazol-2-yl)phenyl]-3,3'p-phenylene-bis-acrylamide dihydrochloride (GW4869) was obtained from Cayman CHEMICAL (Ann Arbor, MI, USA). Cell lines including, Huh-7 hepatoblastoma cells, non-small cell lung cancer cells (A549) and breast cancer cells (MDA-MB-231) were purchased from ATCC (Manassas, VA, USA). Materials to build the size-based exosome isolation platform (ExoTIC [20]) were obtained from McMaster-Carr (Los Angeles, CA,

USA), Cytiva (Marlborough, MA, USA) and Sterlitech (Kent, WA, USA). Culture media for HUVEC cells were obtained from PromoCell GmbH (Heidelberg, Germany).

**Preparation of nanovesicles.** The detailed procedures for synthesizing 100nm liposomes with different lipid membrane compositions, preparation of EVs from mouse hepatocytes with embedded green fluorescent protein, EVs from human hepatocellular carcinoma (HuH-7), and EVs from HUVEC and MDA-MB-231 cell lines are presented in Supporting Information under Methods.

Device assembly and electrical impedance measurements. The device consists of two modules: a micropipette-based dielectrophoretic device for entrapment of the vesicles and a digital impedance analyzer setup for *in situ* impedance measurements of the trapped vesicles. The fabrication procedure of micropipette-based dielectrophoretic device has been previously reported by our group [18,19,21]. After assembling the device,  $10~\mu$ L PBS solution and  $10~\mu$ L PBS solution containing the vesicles at concentration of  $6.55\times10^6$  particles/ $\mu$ L were injected into chambers to immerse the base side and tip side of the pipette respectively. A set of platinum electrodes with 0.51~mm in diameter was placed into the chambers to apply 10~V/cm DC across the pipette for 5~minutes. The entrapment of the particles was simultaneously observed and recorded using an inverted microscope (TE2000-S, Nikon Instruments) and a high-resolution camera (Andor NeoZyla 5.5, Oxford Instruments) at a capture rate of 100~frames/second.

A digital impedance analyzer (HF2LI, Zurich Instruments) was connected to the second set of platinum electrodes with 130  $\mu$ m diameter. The electrodes were precisely placed across the trapped particles 20  $\mu$ m apart via a multi-micromanipulator system (MPC-200, Sutter Instrument Company). The impedance of the trapped particles was measured as an AC field with a peak amplitude of 100 mV swept from 0.5 MHz to 50 MHz. Frequency-based logarithmic sweep mode was used to record the amplitude and phase of the impedance signal to generate the impedance spectrum. In order to obtain magnitude opacity values at frequencies of interest, we generated a polynomial curve fit of measured impedance spectrum using the MATLAB function Polyfit. The magnitude opacity values were extracted based on the fitted polynomial function.

For statistical analysis, impedance measurement of each sample was repeated for at least 15 times unless otherwise noted and the results were presented as average and standard deviation. Two-sample t-tests were performed to compare the two population means, where value P < 0.05 (\*\*) was considered as the statistical significance [22].

#### 3. Results and Discussion

Studies have shown that the impedance of cells under AC field exhibits variation as a function of frequency. Generally, at low range of frequency (~kHz), cells are insulating and resisting the current flowing into their interior and thus, the impedance is dominated by the cell's volume. As the frequency increases (>1MHz), the cell's membrane exhibits a capacitive response due to the polarization of the interface between their membrane and surrounding medium; hence, the impedance is influenced by the membrane capacitance. At higher frequencies (>10MHz), the electric field (E-field) can penetrate through the cell membrane and polarize the cytoplasm; and thus, the impedance reflects the cytosolic conductance of the cell [12]. However, other studies have also shown different frequency responses for phospholipid vesicles with smaller diameters, which reflects their size, surface charge as well as dielectric properties of their membrane and cytosol [12,23]. Here, we investigated the impedance of a cluster of EVs harvested from different parental cells or cells cultured in different culture conditions at a wide range of frequency (0.5MHz to 50 MHz) to detect EVs based on their unique dielectric properties.

# 3.1. Magnitude opacity

The impedance signal was reported to be influenced by the concentration of entrapped particles [24]. This effect, to some extent, could be compensated by presenting the

impedance signal as magnitude opacity represented in Eq (1). Magnitude opacity O(f) is defined as a ratio of the impedance at all frequencies Z(f) to the impedance  $Z(f_{reference})$  measured at a size dependent reference frequency (eg. 0.5MHz) [25]. This concept has been widely applied in cell cytometry to normalize the impedance signal with respect to the cell size and its relative position to the electrodes [26,27]. Thus, the opacity, O(f), a volume-independent parameter, would mostly reflect the impedance response of the EVs in terms of their dielectric properties.

$$O(f) = \frac{Z(f)}{Z(f_{reference})} \tag{1}$$

To verify that the magnitude opacity provides information about the dielectric properties of vesicles, cluster of liposomes at two different concentrations were analyzed. We have previously showed that our device is capable of trapping more vesicles in a form of clusters as the duration of applied E-field increased [19]. Thus, 100 nm liposomes were trapped by applying 10 V/cm E-field for 2- and 5-minutes intervals. Microscopic images (Figure 2a) showed a higher concentration of liposomes was collected after applying the voltage for 5 minutes (Figure 2a ii) compared to 2 minutes entrapment interval (Figure 2a i). The number of trapped liposomes were quantified as 2.2×106 for 2 minutes and 5.4×106 for 5 minutes entrapment after releasing them into 10 µL fresh PBS buffer, followed by nanoparticle tracking analysis (NTA) [18]. The impedances of two clusters were normalized to obtain the magnitude opacity, and the results were compared with impedance of the system without liposomes (Before entrapment) (Figure 2b and Figure S5). The result indicated no statistically significant difference (P > 0.05) between the two concentrations of entrapped liposomes, while they are significantly different from the impedance of the system without any liposomes. This experiment was repeated with COOH-PS beads and other particles of similar size distribution to validate the magnitude opacity analysis (data not shown). The overlapped magnitude opacity of liposomes at two intervals suggested that the opacity concept can be utilized to mainly analyze the dielectric properties of the vesicles despite their cluster size.

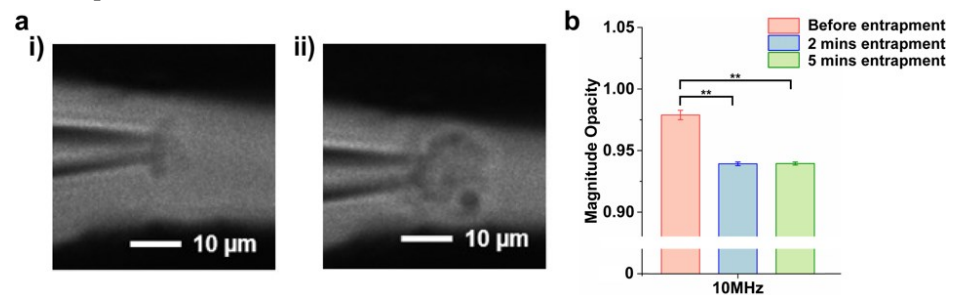


**Figure 2. (a)** Microscopic images of liposomes entrapment for **i)** 2 minutes with the average number of trapped vesicles as  $2.2 \times 10^6$  and **ii)** 5 minutes with the average number of trapped vesicles as  $5.4 \times 10^6$ ; **(b)** The magnitude opacity comparison among empty pipette (before entrapment) and liposome clusters extracted at two different time intervals at 10MHz. \*\*P < 0.05

#### 3.2. Detection of nanoparticles with known dielectric properties

To verify the concept of impedance spectroscopy for nano-size particles, liposomes with known dielectric properties were synthesized and measured, and a mathematical model was constructed based on an equivalent circuit to support the empirical results. Two sets of 100 nm liposomes were synthesized with different membrane compositions as molar ratios of L- $\alpha$ -Phosphatidylcholine (PC) and cholesterol (CH) were changed from 10 to 1 and 1 to 10 ratios: CH:PC(1:10) and CH:PC(10:1) shown in Figure 3a. The capacitance and resistance of the PC lipid bilayer were reported in the literature as 0.38  $\mu F/cm^2$ , 1.44×  $10^4 \Omega \cdot cm^2$ , and CH bilayer as 0.61  $\mu F/cm^2$ , 2.12×  $10^6 \Omega \cdot cm^2$  by an electrochemical impedance spectroscopy [28]. Similar sized COOH- PS beads were selected as a reference particle on the basis of their relatively explicit dielectric property.

The customized mathematical model was built for the cluster of liposomes and — COOH-PS beads suspended in PBS buffer, which is described in detail in the supporting information. In brief, the impedance of the particles ( $Z_{\rm mix}$ ) was estimated by firstly extracting the particles' permittivity and conductivity based on the capacitance and resistance of membrane and inner medium to obtain the complex permittivity  $\tilde{\varepsilon}_{mix}$ , followed by estimating  $Z_{\rm mix}$  using Maxwell's mixture equation [12]. The estimated  $Z_{\rm mix}$  was implemented into the equivalent circuit to calculate the impedance of the system. The mathematical estimation of particles' impedance at a wide frequency range was presented as magnitude opacity spectrum. It is important to note that a quantitative comparison on magnitude opacity values between the empirical results and the values obtained from the mathematical model is not exact; since the mathematical model has been simplified and the impedance could potentially be influenced by other factors such as non-ideal characteristics of the measurement electronics [26,29]. Thus, we mainly focus on the comparison between the relative differences in particles' impedance obtained from empirical and mathematical results, rather than their exact values.

Figure 3b represents the magnitude opacity obtained by the mathematical model of liposomes with different compositions and COOH-PS beads. Due to enriched content of highly resistive cholesterol in liposomes with CH:PC(10:1), higher opacity was obtained when compared to liposomes with CH:PC(1:10) composition. Beads have lower magnitude opacity than liposomes, as previously reported by our group, owing to their negatively charged carboxylic acid functional groups [24]. Figure 3c shows the empirical comparison of magnitude opacity for the same particles. A clear difference was also observed empirically for liposomes with different compositions; and the CH:PC(10:1) liposome showed higher magnitude opacity when compared to the CH:PC(1:10) liposomes, which was in agreement with the theoretical model (Figure 3b). These comparisons illustrate that our impedance system is capable of discriminating between particles based on the difference in their membrane compositions.

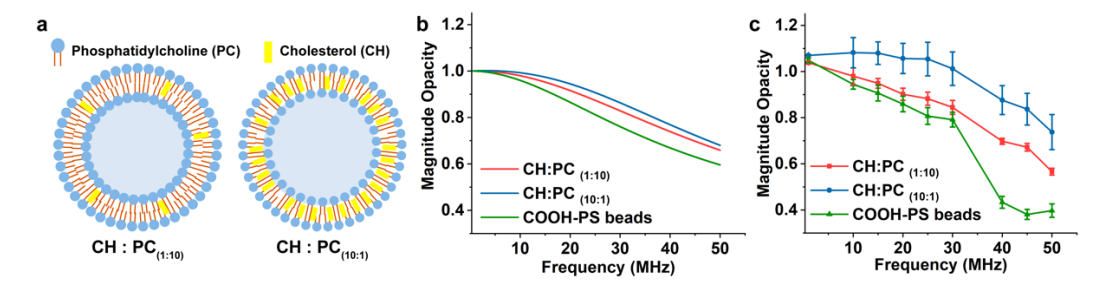


**Figure 3. (a)** Schematic representations of two types of liposomes with different membrane compositions (CH:PC<sub>(1:10)</sub> and CH:PC<sub>(10:1)</sub>); The relative magnitude opacity of liposomes and COOH-PS beads (average size of all particles are 100 nm) utilizing **(b)** the mathematical model and **(c)** the experimental measurement.

# 3.3. Detection of EVs with different membrane compositions

The EIS was further utilized to investigate the difference between EVs with different membrane compositions. EVs derived from primary hepatocytes were engineered to have green fluorescent protein (GFP+) embedded in their membrane and were compared to the EVs harvested from wild type , lacking the GFP protein (GFP-) [30]. We postulated that the localization of GPF in the membrane of EVs would lead to the alternation of their dielectric properties which would be detected by EIS. The magnitude opacity spectrum of two EVs are shown in Figure 4a. Results showed detectable opacity when compared GFP-and GFP+ EVs at frequencies higher than 10 MHz (Figure 4b and Figure S8). Although the differences between the opacity of EVs are relatively small here, we have observed consistent results when various batches of EVs were measured at different time points and we believe the relatively low sensitivity of the detected opacity can be further improved

by reducing the dimensions of sensing electrodes at fixed positions in our integrated device in future studies. The lower magnitude opacity of GFP+ EVs compared to the wild type (GFP-) could most likely be due to an increase in the membrane conductivity as a result of the incorporated charged green fluorescent proteins. Also, the relative opacity of EVs with different membrane compositions is in agreement with the relative opacity spectrum obtained from liposomes with different lipid membrane contents as described above; suggesting that the system could potentially detect nanovesicles with different membrane compositions at intermediate to high frequency range

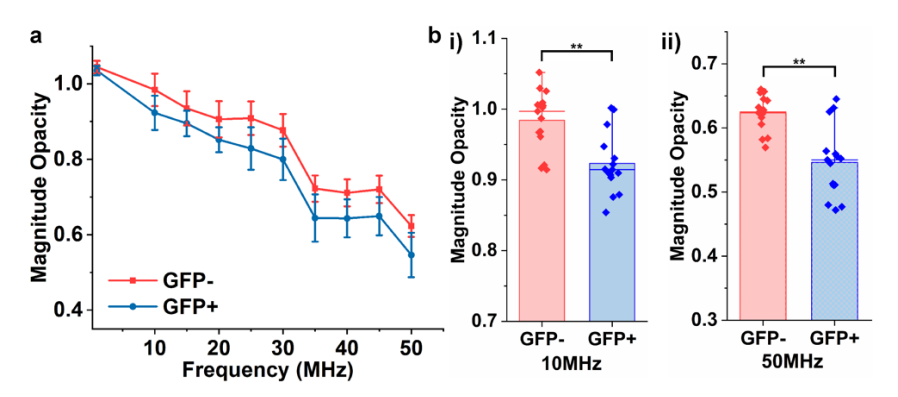


**Figure 4. (a)** The magnitude opacity spectrum of EVs derived from wild-type primary hepatocytes (GFP-) and GPF+ hepatocytes. **(b)** Significant difference in magnitude opacity was observed at 10MHz and higher frequencies up to 50MHz. \*\**P*<0.05

## 3.4. Detection of EVs secreted from cells treated under different culture conditions

EVs with diverse membrane and cytosolic compositions were selected by harvesting them from human hepatocellular carcinoma cell lines under different culture conditions (Figure 5a). Palmitate acid (PA) a pro-inflammatory fatty acid that can stimulate hepatocytes to generate pro-inflammatory EVs [31] was added in the culture media. PA also reported to cause variations on EVs' lipidomic and miRNA expression profiles [32]. Sphingomyelin phosphodiesterase 3 (SMPD 3) specific inhibitor (GW4869) was reported as a neutral inhibitor of sphingomyelinase to attenuate the inflammatory effect in cells [33]. Cells were cultured under the mixture of PA and GW4869 and the harvested EVs were compared to EVs extracted from cells treated with PA treated culture condition. EVs collected from cells under no stimulus was selected as a blank control. The inflammatory response of EVs collected from these three conditions were examined by culturing EVs with mouse bone marrow-derived macrophages (BMDM); and analyzed for the cytokines Interleukin 6 (IL-6) and tumor necrosis factor alpha (TNF- $\alpha$ ) mRNA expression levels via quantitative polymerase chain reaction (q-PCR) (Figure 5b). Results showed significantly elevated expression levels of TNF- $\alpha$  and IL-6 mRNAs, reflecting the inflammatory responses of EVs derived from PA-treated culture condition. GW4869 inhibited the inflammatory effect caused by PA, and thus, EVs harvested from cells treated with the mixture of PA and GW4869 resulted in reduction of mRNA expression levels of TNF- $\alpha$  and IL-6.

Given the potential variations in the biochemical properties of EVs harvested from cells under the pro-inflammatory stimulus, EVs dielectric properties were studied by EIS (Figure 5c). EVs harvested from PA-treated condition showed elevated magnitude opacity at 10MHz when compared to EVs harvested from cells treated with mixture of PA and GW which could potentially be due to the increase of ceramide lipids in EVs' membrane composition under PA-tread condition [34]. Since the capacitance of ceramide lipid bilayer is lower than the phosphatidylcholine bilayer [35], EVs containing higher concentration of ceramide lipid will have a lower membrane capacitance, resulting in higher magnitude opacity when compared to PA+GW treated EVs. However, as frequency increased to 20MHz and above, the opacity of EVs treated with PA became lower than both the control and PA+GW treated EVs. This shift in opacity, could be related to the dominant

315

316

317

318

319

320

321

322

323

324

325

326

327

328

329

330

331

332

333

334

335

336

337

338

339

340

341

342

343

role of cytosolic properties at high frequency range [36]. Overexpressed RNA in PA treated EVs leads to the reduction of cytosolic resistance and hence, reduction of magnitude opacity [32].

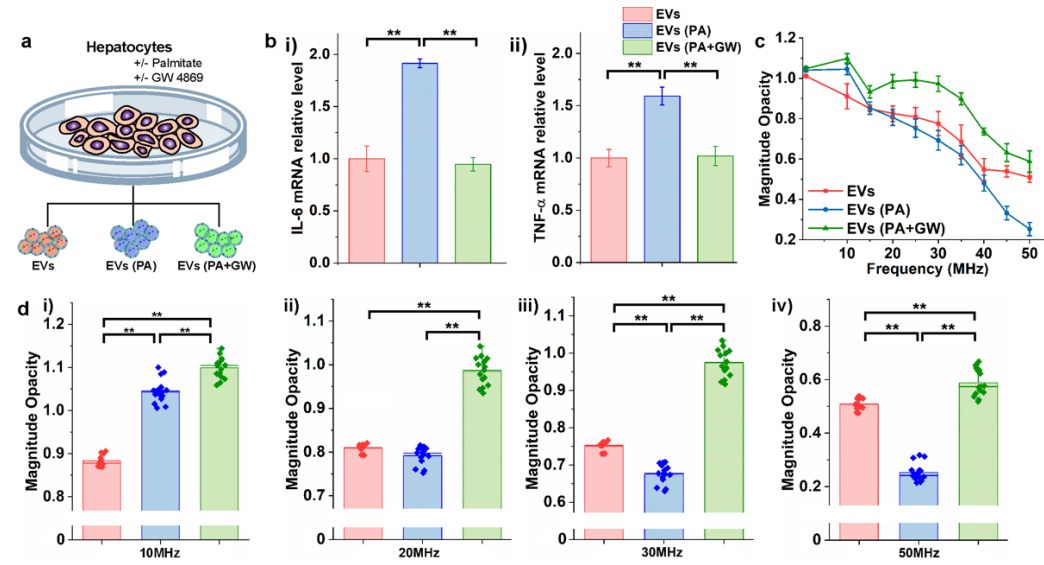


**Figure 5. (a)** Isolation of EVs from human hepatocellular carcinoma cell lines under: normal culture medium, PA treated condition and the mixture of PA and GW4869 treated conditions. **(b)** Mouse Bone-marrow-derived macrophage (BMDM) were cultured with EVs for mRNA expression analysis by the quantitative polymerase chain reaction of **i)** IL-6 mRNA and **ii)** TNF- $\alpha$  mRNA; **(c)** Magnitude opacity spectrum of EVs derived from human hepatocellular carcinoma cell lines under three culture conditions. **(d)** Bar plots of magnitude opacity comparison of EVs at three culture conditions at 10MHz - 50MHz. \*\*P<0.05

# 3.5. Differentiating EVs from lipoproteins

We further utilized the EIS to discriminate EVs from lipoproteins which share similarities in biophysical properties but have different biochemical properties. Lipoproteins have single layer phospholipids embedded with apolipoproteins, and are in charge of the transportation of water-insoluble hydrophobic lipid molecules into extracellular fluids [37]. Although both lipoproteins and EVs have embedded proteins in their membrane structure, studies have shown that they have diverse lipid and membrane protein compositions [38], which could potentially lead to variations of their dielectric properties. In addition, lipoproteins encapsulate hydrophobic lipid molecules including triglyceride (TG) and cholesterol in their lumen, while EVs have high concentration of charged proteins. The impedance of EVs derived from A549 NSCLC cells and very low-density (VLD) lipoproteins from human plasma was measured under wide frequency spectrum (Figure 6a). The difference between their opacity became significant at frequencies above 10MHz (Figure 6b and Figure S9). The opacity of EVs was relatively lower than the VLDL which could be attributed to the higher concentration of overall charged molecules, including proteins and nucleic acids, embedded in their membrane and lumen. However, to precisely correlate the membrane and cytosolic composition of nanovesicles to their frequency-dependent impedance, molecular analysis of vesicles such as proteomic, lipidomic and genomic, need to be performed which will be the subject of our future studies.

**Figure 6. (a)** Magnitude opacity spectrum of EVs derived from A549 non-small cell lung cancer (NSCLC) cell line and very low-density (VLD) lipoprotein. **(b)** Bar plots of magnitude opacity comparison of NSCLC and VLD lipoproteins at 10MHz and 50MHz. \*\*P<0.05

#### 3.6. Detection of EVs derived from different cellular origins

Detection of EVs' dielectric properties harvested from different cellular origins is of particular interest since the secreted EVs could provide essential biochemical information including nucleic acids and protein contents, about the parental cells [39]. Here, we utilized EVs harvested from two common cell lines, umbilical vein endothelial cells (HU-VEC) and epithelial human breast cancer (MDA-MB-231), to investigate their differences by EIS. EVs secreted from MDA-MB-231 cells are widely studied for its enriched oncogenes in the lumen which lead to the oncogenic transformation [40]. HUVEC cell line were commonly used to study the role of angiogenic EVs secreted from MDA-MB-231 cell line in tumor growth and metastasis [41]. When compared the impedance of EVs derived from these two cell lines, significantly higher magnitude opacity was observed for MDA-MB-231 derived EVs at frequencies 10MHz to 20MHz (Figure 7a). However, as the frequency increased above 20 MHz, the difference between their opacities became insignificant (at 30 MHz and 40MHz) and as the frequency reached to 50MHz, the opacity of EVs derived from HUVEC exceeded the EVs harvested from MDA-MB-231 cells. Given the previous observations, we postulated that the shift in magnitude opacity at frequency above 30MHz could potentially be caused by a dominant effect of cytosolic conductance in EVs, and as a result it overturned the difference in opacity caused by their membrane capacitance. Although these initial observations provide an insight with regards to EVs' cytosolic and membrane effect on their dielectric properties at different range of the frequency spectrum, more compressive and precise studies on EVs' molecular profiles need to be conducted to correlate the exact role of membrane and cytosol on their frequency-dependent dielectric properties which will be the subject of our future studies.

#### 3.7. Detection of EVs of different size distribution

Besides the effect of parental cells on EVs biochemical and biophysical characteristics, the heterogeneity of EVs in their size also adds to the complexity of their characterization [42]. It has been reported that EVs have different biochemical properties including protein, lipid and nucleic acid contents, at different size range [43,44]. For instance, Zhang et al. showed that EVs derived from MDA-MB-231 cell line at different sizes have different biochemical and biophysical properties including zeta potential, stiffness, lipid composition, proteomic and nucleic acid payload [43]. Thus, we measured the impedance of EVs derived from MDA-MB-231 cell line at different size distributions to investigate the correlation of EVs' size to their dielectric properties. EVs derived from MDA-MB-231 cells were isolated utilizing a size-based sorting platform- ExoTIC developed by our group [20]. Figure 7bi showed the magnitude opacity spectrum of EVs at different size range, and the results illustrated significant difference between each group of EVs (Figure 7b ii, iii and S10). Although this preliminary data provides an important information with regards to the correlation of EVs size distribution and their dielectric properties, it is not

348

349

350

351

352

353

354

355

356

357

358

359

360

371

feasible to report the exact causes of their impedance differences; given the fact that each subpopulation is different in more than one biophysical and/or biochemical parameter. Thus, the EIS can be utilized as a tool to provide a rapid detection between EVs of different size, and a comprehensive downstream analysis on EVs' molecule profile will be required to further study the effects of their membrane or cytosolic cargos.

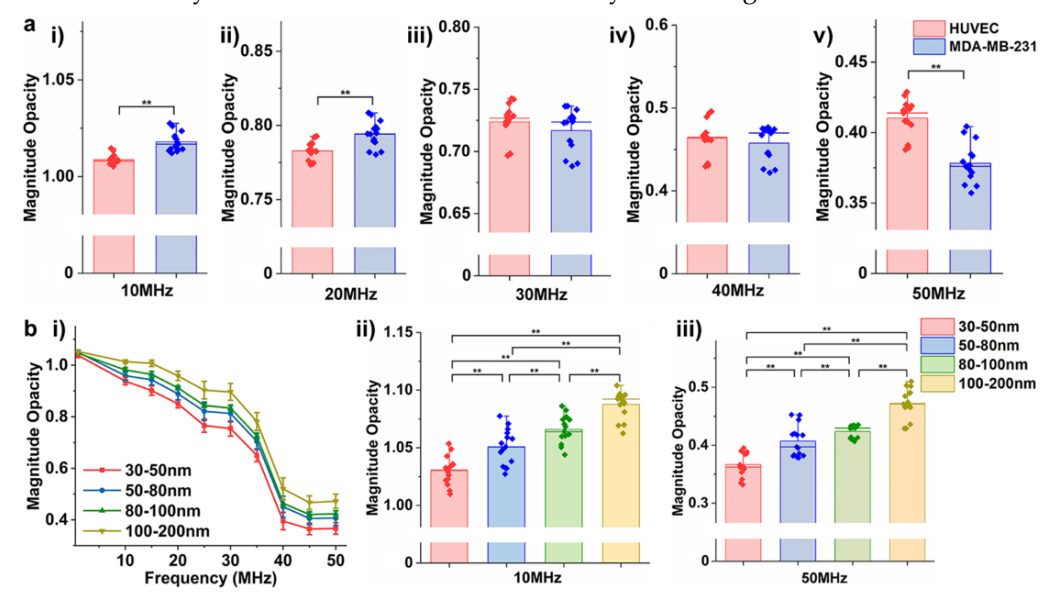


**Figure 7.** The magnitude opacity comparison of EVs extracted from **(a)** Human umbilical vein endothelial cells (HUVEC) and epithelial human breast cancer (MDA-MB-231) cells. \*\*P<0.05 **(b) i)** Magnitude opacity spectrum of EVs at different size range isolated from MDA-MB-231 cell line by ExoTIC. **ii-iii)** Bar plots of magnitude opacity comparison of four EVs subsets at 10MHz and 50MHz. \*\*P<0.05

#### 4. Conclusions

In summary, this study has reported a label-free biosensor for detection of EVs based on their unique dielectric properties. The system consisted of a micropipette-based dielectrophoretic device integrated with an EIS to measure the impedance of immobilized vesicles at a wide range of frequency. The detection principle was mathematically modeled based on an equivalent circuit and was in agreement with empirical results when nanovesicles with known dielectric properties were tested. Also, the system showed that EVs could be discriminated from lipoproteins, which shared similar biophysical properties but differed in their biochemical compositions. Moreover, EVs with different membrane compositions but the same cytosolic contents were detected by the platform at frequencies above 10MHzIn addition, the impedance of EVs harvested from cells in different culture conditions and thus, different functionality in terms of pro-inflammatory effect were detected at intermediate and high frequency range (10 MHz to 50 MHz).

Furthermore, the sensor could detect EVs derived from different cellular origins, which could be further utilized to rapidly characterize EVs in diagnostic and therapeutic applications. We also illustrated the capability of the EIS to differentiate EVs at different size distributions, which presented the heterogeneity of their dielectric properties associated with their biochemical properties. Overall, this novel biosensor opens up a new way for rapid, label-free, and non-invasive EVs characterization based on their unique dielectric properties which can be associated with their charge-dependent membrane and cytosolic molecular contents. This technique also holds a great potential to be further evolved as a diagnostic tool for detection of pathogenic EVs, and can be applied for monitoring the EVs' cargos in personalized therapeutics.

422

423

424

425

426

427

428

429

430

431

432

433

434

435

436

437

438

439

440

441

442

443

444

445

446

447

448

449

450

451

452

453

454

455

456

457

458

459

460

461

462

463

464

465

467

468

470

471

472

473

474

Supplementary Materials: The following supporting information can be downloaded at: www.mdpi.com/xxx/s1, Figure S1: (a) NTA results of liposomes CH:PC(1:10) (b) NTA result of liposomes CH:PC(10:1) synthesized by extrusion method.; Figure S2. (a) An in vivo strategy to label EVs with GFP in a hepatocyte-specific manner. Recombination results in an inversion, and the region between the lox66-lox71 sites is reversed. EVtS-GFP can be expressed under the control of Cre-recombinase. (b) EXtS-GFP line was breeding with albumin-cre mice (EXtS-GFPAlb-cre mice); Microscopy image showed the representative patterns of GFP expression in liver cells; (c) i) Extracellular vesicles were collected from the conditioned medium of primary hepatocytes from EVtS-GFP mice (Alb-Cre negative and positive); ii) Western blot analysis of GFP in collected EVs and lysates. The Flotillin-2/Flot2 was used as an EV marker; Figure S3. NTA results of EVs extracted from culture media of (a) control (b) green fluorescent protein (GFP+) transgenic mouse primary hepatocytes; Figure S4. NTA results of EVs extracted from culture medium of HuH-7 cell lines (a) control (b) palmitate acid (c) mixture of palmitate acid and GW4869; Figure S5. Experimental data showing the magnitude opacity comparison among empty pipette (before entrapment) and liposome clusters extracted at two different time intervals at 20MHz-50MHz. \*\*P<0.05; Figure S6. (a) An equivalent circuit model for the impedance measurement system. Liposomes in suspension are modeled as a capacitor Cp (membrane) and a resistor Rp (cytoplasm) in series based on the Foster and Schwan's simplified circuit model; (b) A magnitude opacity spectrum that exemplifies impedance shifts (dash lines) upon a resistance change ( $\Delta R_P$ ) and capacitance change ( $\Delta C_P$ ) of particles; (c) Diagram of a single-shell model, representing a single vesicle in suspension. εm and σm represent the permittivity and conductivity of the medium;  $\epsilon_{mem}$  and  $\sigma_{mem}$  depict the permittivity and conductivity of the membrane;  $\varepsilon_i$  and  $\sigma_i$  describe the permittivity and conductivity of the lumen; Figure S7. Schematic diagram of the HF2LI impedance analyzer. Rin (50  $\Omega$ ) and Rs (50  $\Omega$ ) are intrinsic resistors coupled in the impedance analyzer. Zmix represents the impedance of the particle cluster, and Vin is the input voltage (0.1V); Figure S8. The magnitude opacity comparison of EVs derived from wild type primary hepatocytes (GFP-) and GPF+ hepatocytes at 20MHz-40MHz. \*\*P<0.05; Figure S9. Magnitude opacity comparison of EVs derived from A549 non-small cell lung cancer (NSCLC) cell line and very low-density (VLD) lipoprotein at 20MHz-40MHz. \*\*P<0.05; Figure S10. The magnitude opacity of EVs derived from MDA-MB-231 cell line with different size range measured at 20MHz-40MHz. \*\*P<0.05

**Author Contributions:** Conceptualization, L. E.; Methodology, Y. Z., K. M., V.J. B. and M.O. O; Software, Y. Z.; Validation, Y. Z.; Formal Analysis, Y. Z.; Investigation, L. E. and Y. Z.; Resources, Y. Z., T. N., K. M., V.J. B., M.O. O, U. D. and L. E.; Data Curation, Y. Z.; Writing – Original Draft Preparation, Y. Z.; Writing – Review & Editing, L. E., T. N., M.O. O and U. D.; Visualization, Y. Z.; Supervision, L. E.; Project Administration, L. E.; Funding Acquisition, L. E. and T. N.. All authors have read and agreed to the published version of the manuscript.

**Funding:** This work was funded by NSF EAGER ECCS (2020112), NSF CAREER ECCS (2046037), R21 (CA240664), R01 (DK123181), and Department of Pediatrics of Defense (W81XWVH1910038).

**Acknowledgments:** The author thanks L. Shi for the generous assistant on developing insulator-based dielectrophoretic trapping system and S. M. Shahid on impedance data analysis.

Conflicts of Interest: U. Demirci is a founder of and has an equity interest in: (i) DxNow Inc., a company that is developing microfluidic IVF tools and imaging technologies for point of-care diagnostic solutions, (ii) Koek Biotech, a company that is developing microfluidic technologies for clinical solutions, (iii) Levitas Inc., a company focusing on developing microfluidic products for sorting rare cells from liquid biopsy in cancer and other diseases, and (iv) Hillel Inc., a company bringing microfluidic cell phone tools to home settings.

# References

- 1. Pegtel, D.M.; Gould, S.J. Exosomes. *Annu. Rev. Biochem.* 2019, 88, 487-514, doi:10.1146/annurev-biochem-013118-111902.
- 2. He, C.; Zheng, S.; Luo, Y.; Wang, B. Exosome Theranostics: Biology and Translational Medicine. *Theranostics*. 2018, 8, 237-255, doi:10.7150/thno.21945.
- 3. van der Pol, E.; Böing, A.N.; Harrison, P.; Sturk, A.; Nieuwland, R. Classification, Functions, and Clinical Relevance of Extracellular Vesicles. *Pharmacol Rev.* 2012, 64, 676, doi:10.1124/pr.112.005983.
- 4. Azmi, A.S.; Bao, B.; Sarkar, F.H. Exosomes in cancer development, metastasis, and drug resistance: a comprehensive review. *Cancer Metastasis Rev.* 2013, 32, 623-642, doi:10.1007/s10555-013-9441-9.

- 5. Yamashita, T.; Takahashi, Y.; Nishikawa, M.; Takakura, Y. Effect of exosome isolation methods on physicochemical properties of exosomes and clearance of exosomes from the blood circulation. *Eur. J. Pharm. Biopharm.* 2016, 98, 1-8, doi:https://doi.org/10.1016/j.ejpb.2015.10.017.
- 6. Zhang, W.; Peng, P.; Kuang, Y.; Yang, J.; Cao, D.; You, Y.; Shen, K. Characterization of exosomes derived from ovarian cancer cells and normal ovarian epithelial cells by nanoparticle tracking analysis. *Tumor. Biol.* 2016, 37, 4213-4221, doi:10.1007/s13277-015-4105-8.
- 7. Atay, S.; Gercel-Taylor, C.; Kesimer, M.; Taylor, D.D. Morphologic and proteomic characterization of exosomes released by cultured extravillous trophoblast cells. *Exp. Cell Res.* 2011, 317, 1192-1202, doi:https://doi.org/10.1016/j.yexcr.2011.01.014.
- 8. Van Der Pol, E.; Van Gemert, M.J.C.; Sturk, A.; Nieuwland, R.; Van Leeuwen, T.G. Single vs. swarm detection of microparticles and exosomes by flow cytometry. *J. Thromb. Haemost.* 2012, 10, 919-930, doi:10.1111/j.1538-7836.2012.04683.x.
- 9. de Rond, L.; van der Pol, E.; Bloemen, P.R.; Van Den Broeck, T.; Monheim, L.; Nieuwland, R.; van Leeuwen, T.G.; Coumans, F.A.W. A Systematic Approach to Improve Scatter Sensitivity of a Flow Cytometer for Detection of Extracellular Vesicles. *Cytometry A.* 2020, 97, 582-591, doi:10.1002/cyto.a.23974.
- 10. Simpson, R.J.; Jensen, S.S.; Lim, J.W.E. Proteomic profiling of exosomes: Current perspectives. *Proteomics*. 2008, 8, 4083-4099, doi:10.1002/pmic.200800109.
- 11. Schade-Kampmann, G.; Huwiler, A.; Hebeisen, M.; Hessler, T.; Di Berardino, M. On-chip non-invasive and label-free cell discrimination by impedance spectroscopy. *Cell Prolif.* 2008, 41, 830-840, doi:https://doi.org/10.1111/j.1365-2184.2008.00548.x.
- 12. Sun, T.; Morgan, H. Single-cell microfluidic impedance cytometry: a review. *Microfluid. Nanofluid.* 2010, 8, 423-443, doi:10.1007/s10404-010-0580-9.
- 13. Bagnaninchi, P.O.; Drummond, N. Real-time label-free monitoring of adipose-derived stem cell differentiation with electric cell-substrate impedance sensing. *Proc. Natl. Acad. Sci.* 2011, 108, 6462, doi:10.1073/pnas.1018260108.
- 14. Cho, Y.; Kim, H.S.; Frazier, A.B.; Chen, Z.G.; Shin, D.M.; Han, A. Whole-Cell Impedance Analysis for Highly and Poorly Metastatic Cancer Cells. *J. Microelectromech. Syst.* 2009, 18, 808-817, doi:10.1109/JMEMS.2009.2021821.
- 15. Zhou, Y.; Basu, S.; Laue, E.; Seshia, A.A. Single cell studies of mouse embryonic stem cell (mESC) differentiation by electrical impedance measurements in a microfluidic device. *Biosens. Bioelectron.* 2016, 81, 249-258, doi:https://doi.org/10.1016/j.bios.2016.02.069.
- 16. Song, H.; Wang, Y.; Rosano, J.M.; Prabhakarpandian, B.; Garson, C.; Pant, K.; Lai, E. A microfluidic impedance flow cytometer for identification of differentiation state of stem cells. *Lab Chip*. 2013, 13, 2300-2310, doi:10.1039/C3LC41321G.
- 17. Holmes, D.; Pettigrew, D.; Reccius, C.H.; Gwyer, J.D.; van Berkel, C.; Holloway, J.; Davies, D.E.; Morgan, H. Leukocyte analysis and differentiation using high speed microfluidic single cell impedance cytometry. *Lab Chip.* 2009, 9, 2881-2889, doi:10.1039/B910053A.
- 18. Shi, L.; Kuhnell, D.; Borra, V.J.; Langevin, S.M.; Nakamura, T.; Esfandiari, L. Rapid and label-free isolation of small extracellular vesicles from biofluids utilizing a novel insulator based dielectrophoretic device. *Lab Chip.* 2019, 19, 3726-3734, doi:10.1039/C9LC00902G.
- 19. Shi, L.; Rana, A.; Esfandiari, L. A low voltage nanopipette dielectrophoretic device for rapid entrapment of nanoparticles and exosomes extracted from plasma of healthy donors. *Sci. Rep.* 2018, 8, 6751, doi:10.1038/s41598-018-25026-2.
- 20. Liu, F.; Vermesh, O.; Mani, V.; Ge, T.J.; Madsen, S.J.; Sabour, A.; Hsu, E.-C.; Gowrishankar, G.; Kanada, M.; Jokerst, J.V.; et al. The Exosome Total Isolation Chip. ACS Nano 2017, 11, 10712-10723, doi:10.1021/acsnano.7b04878.
- 21. Zhang, Y.; Rana, A.; Stratton, Y.; Czyzyk-Krzeska, M.F.; Esfandiari, L. Sequence-Specific Detection of MicroRNAs Related to Clear Cell Renal Cell Carcinoma at fM Concentration by an Electroosmotically Driven Nanopore-Based Device. *Anal. Chem.* 2017, 89, 9201-9208, doi:10.1021/acs.analchem.7b01944.
- 22. Krzywinski, M.; Altman, N. Significance, P values and t-tests. Nat. Methods 2013, 10, 1041-1042, doi:10.1038/nmeth.2698.
- 23. Di Biasio, A.; Ambrosone, L.; Cametti, C. The dielectric behavior of nonspherical biological cell suspensions: an analytic approach. *Biophys. J.* 2010, 99, 163-174, doi:10.1016/j.bpj.2010.04.006.
- 24. Shi, L.; Esfandiari, L. An Electrokinetically-Driven Microchip for Rapid Entrapment and Detection of Nanovesicles. *Micromachines*. 2021, 12, doi:10.3390/mi12010011.
- 25. Hoffman, R.A.; Johnson, T.S.; Britt, W.B. Flow cytometric electronic direct current volume and radiofrequency impedance measurements of single cells and particles. *Cytometry* 1981, 1, 377-384, doi:10.1002/cyto.990010605.
- 26. Haandbæk, N.; Bürgel, S.C.; Heer, F.; Hierlemann, A. Characterization of subcellular morphology of single yeast cells using high frequency microfluidic impedance cytometer. *Lab Chip.* 2014, 14, 369-377, doi:10.1039/C3LC50866H.
- 27. Norlin, A.; Pan, J.; Leygraf, C. Investigation of interfacial capacitance of Pt, Ti and TiN coated electrodes by electrochemical impedance spectroscopy. *Biomol. Eng.* 2002, 19, 67-71, doi:https://doi.org/10.1016/S1389-0344(02)00013-8.
- 28. Naumowicz, M.; Petelska, A.D.; Figaszewski, Z.A. Capacitance and resistance of the bilayer lipid membrane formed of phosphatidylcholine and cholesterol. *Cell. Mol. Biol. Lett.* 2003, 8, 5-18.
- 29. Gawad, S.; Schild, L.; Renaud, P. Micromachined impedance spectroscopy flow cytometer for cell analysis and particle sizing. *Lab Chip.* 2001, 1, 76-82, doi:10.1039/B103933B.
- 30. Yim, N.; Ryu, S.-W.; Choi, K.; Lee, K.R.; Lee, S.; Choi, H.; Kim, J.; Shaker, M.R.; Sun, W.; Park, J.-H.; et al. Exosome engineering for efficient intracellular delivery of soluble proteins using optically reversible protein–protein interaction module. *Nat. Commun.* 2016, 7, 12277, doi:10.1038/ncomms12277.

- 31. Nakamura, S.; Takamura, T.; Matsuzawa-Nagata, N.; Takayama, H.; Misu, H.; Noda, H.; Nabemoto, S.; Kurita, S.; Ota, T.; Ando, H.; et al. Palmitate Induces Insulin Resistance in H4IIEC3 Hepatocytes through Reactive Oxygen Species Produced by Mitochondria\*. *J. Biol. Chem.* 2009, 284, 14809-14818, doi:https://doi.org/10.1074/jbc.M901488200.
- 32. Lee, Y.-S.; Kim, S.Y.; Ko, E.; Lee, J.-H.; Yi, H.-S.; Yoo, Y.J.; Je, J.; Suh, S.J.; Jung, Y.K.; Kim, J.H.; et al. Exosomes derived from palmitic acid-treated hepatocytes induce fibrotic activation of hepatic stellate cells. *Sci. Rep.* 2017, 7, 3710, doi:10.1038/s41598-017-03389-2.
- 33. Essandoh, K.; Yang, L.; Wang, X.; Huang, W.; Qin, D.; Hao, J.; Wang, Y.; Zingarelli, B.; Peng, T.; Fan, G.-C. Blockade of exosome generation with GW4869 dampens the sepsis-induced inflammation and cardiac dysfunction. *Biochim. Biophys. Acta. Mol. Basis. Dis.* 2015, 1852, 2362-2371, doi:https://doi.org/10.1016/j.bbadis.2015.08.010.
- 34. Kakazu, E.; Mauer, A.S.; Yin, M.; Malhi, H. Hepatocytes release ceramide-enriched pro-inflammatory extracellular vesicles in an IRE1 $\alpha$ -dependent manner. *J. Lipid Res.* 2016, 57, 233-245, doi:10.1194/jlr.M063412.
- 35. Naumowicz, M.; Petelska, A.D.; Figaszewski, Z.A. Physicochemical analysis of phosphatidylcholine-ceramide system in bilayer lipid membranes. *Acta Biochim. Pol.* 2008, 55, 721-730, doi: 10.1016/j.redox.2018.101066
- 36. McGrath, J.S.; Honrado, C.; Moore, J.H.; Adair, S.J.; Varhue, W.B.; Salahi, A.; Farmehini, V.; Goudreau, B.J.; Nagdas, S.; Blais, E.M.; et al. Electrophysiology-based stratification of pancreatic tumorigenicity by label-free single-cell impedance cytometry. *Anal. Chim. Acta* 2020, 1101, 90-98, doi:https://doi.org/10.1016/j.aca.2019.12.033.
- 37. Feingold, K.R.; Grunfeld, C. Introduction to lipids and lipoproteins. In endotext [internet]; MDText. com, Inc.: 2018.
- 38. Sun, Y.; Saito, K.; Saito, Y. Lipid Profile Characterization and Lipoprotein Comparison of Extracellular Vesicles from Human Plasma and Serum. *Metabolites* 2019, 9, 259, doi:10.3390/metabo9110259.
- 39. Gurung, S.; Perocheau, D.; Touramanidou, L.; Baruteau, J. The exosome journey: from biogenesis to uptake and intracellular signalling. *Cell Biosci.* 2021, 19, 47, doi:10.1186/s12964-021-00730-1.
- 40. Kruger, S.; Elmageed, Z.Y.A.; Hawke, D.H.; Wörner, P.M.; Jansen, D.A.; Abdel-Mageed, A.B.; Alt, E.U.; Izadpanah, R. Molecular characterization of exosome-like vesicles from breast cancer cells. *BMC Cancer*. 2014, 14, 44, doi:10.1186/1471-2407-14-44.
- 41. Garcia-Hernandez, A.; Leal-Orta, E.; Ramirez-Ricardo, J.; Cortes-Reynosa, P.; Thompson-Bonilla, R.; Salazar, E.P. Linoleic acid induces secretion of extracellular vesicles from MDA-MB-231 breast cancer cells that mediate cellular processes involved with angiogenesis in HUVECs. *Prostaglandins Other Lipid Mediat*. 2021, 153, 106519, doi:https://doi.org/10.1016/j.prostaglandins.2020.106519.
- 42. Gurung, S.; Perocheau, D.; Touramanidou, L.; Baruteau, J. The exosome journey: from biogenesis to uptake and intracellular signalling. *Cell Commun. Signal.* 2021, 19, 1-19, doi: 10.1186/s12964-021-00730-1
- 43. Zhang, H.; Freitas, D.; Kim, H.S.; Fabijanic, K.; Li, Z.; Chen, H.; Mark, M.T.; Molina, H.; Martin, A.B.; Bojmar, L.; et al. Identification of distinct nanoparticles and subsets of extracellular vesicles by asymmetric flow field-flow fractionation. *Nat. Cell Biol.* 2018, 20, 332-343, doi:10.1038/s41556-018-0040-4.
- 44. Kowal, J.; Arras, G.; Colombo, M.; Jouve, M.; Morath, J.P.; Primdal-Bengtson, B.; Dingli, F.; Loew, D.; Tkach, M.; Théry, C. Proteomic comparison defines novel markers to characterize heterogeneous populations of extracellular vesicle subtypes. *Proc. Natl. Acad. Sci.* 2016, 113, E968, doi:10.1073/pnas.1521230113.